Journal of Power Sources 194 (2009) 494–501

Contents lists available at ScienceDirect

Journal of Power Sources

journal homepage: www.elsevier.com/locate/jpowsour

# $Fe^{3+}$ and $Ni^{3+}$ impurity distribution and electrochemical performance of $LiCoO_2$ electrode materials for lithium ion batteries

R. Alcántara [a], G. Ortiz [a], J.L. Tirado [a], R. Stoyanova [b,c,*], E. Zhecheva [b], Sv. Ivanova [b]

[a] Laboratorio de Química Inorgánica, Facultad de Ciencias, Universidad de Córdoba, 14071 Córdoba, Spain
[b] Institute of General and Inorganic Chemistry, Bulgarian Academy of Sciences, 1113 Sofia, Bulgaria
[c] Grenoble High Magnetic Field Laboratory, CNRS, 38042 Grenoble Cedex 9, France

ARTICLE INFO

*Article history:*
Received 8 December 2008
Received in revised form 29 April 2009
Accepted 15 May 2009
Available online 22 May 2009

*Keywords:*
Lithium ion batteries
Cathode materials
Layered oxides
EPR spectroscopy

ABSTRACT

The distribution of $Fe^{3+}$ and $Ni^{3+}$ impurities and the electrochemical performance of $LiCoO_2$ electrodes were examined. Commercial $LiCoO_2$ powders supplied by Aldrich were used. The electrochemical performance of $LiCoO_2$ was modified by rotor blade grinding of $LiCoO_2$ followed by thermal treatment. Structural information on $Fe^{3+}$ and $Ni^{3+}$ impurities was obtained using both conventional X-band and high-frequency electron paramagnetic resonance spectroscopy (EPR). It was found that $Fe^{3+}$ occupies a Co-site having a higher extent of rhombic distortion, while $Ni^{3+}$ is in a trigonally distorted site. After rotor blade grinding of $LiCoO_2$, isolated $Fe^{3+}$ ions display a tendency to form clusters, while isolated $Ni^{3+}$ ions remain intact. Re-annealing of ground $LiCoO_2$ at 850 °C leads to disappearance of iron clusters; isolated $Fe^{3+}$ ions are recovered. The electrochemical performance of $LiCoO_2$ was discussed on the basis of isolated and clustered ions.



## 1. Introduction

As a commercial cathode material for lithium ion batteries, $LiCoO_2$ has been the most widely studied lithium-transition metal oxide during the past decades [1]. The crystal structure of $LiCoO_2$ (space group *R*-3m, α-$NaFeO_2$-type) is composed of a consecutive arrangement of $Li^+$ and $Co^{3+}$ ions in the close-packed oxygen arrays leading to the formation of discrete lithium and cobalt layers [2]. The electrochemical reaction includes a reversible lithium intercalation concomitantly with reversible oxidation of $Co^{3+}$ to $Co^{4+}$ ions [3–6].

The control on the electrochemical performance of $LiCoO_2$ can be achieved by rational manipulation of their structure, morphology and surface. The replacement of $Co^{3+}$ by both electrochemically active and inactive ions (such as $Ni^{3+}$, $Fe^{3+}$, $Mn^{4+}$ [7–12] and $Al^{3+}$, $Ga^{3+}$, $Mg^{2+}$, $Ti^{4+}$ [13–18], respectively) is a way to increase the capacity, to improve the oxide stability in delithiated state and to change the potential of the Li extraction and insertion. $LiCoO_2$ is capable to accommodate a small amount of excess of Li in the Co-layers by creation of oxygen vacancies thus leading to $Li_{1+t}Co_{1-t}O_{2-t}$ with $t \sim 0.04$ [19,20]. The stoichiometric and over-stoichiometric oxides display different reaction mechanism just of in the initial stage of Li extraction. The surface modification of $LiCoO_2$ by coating with oxides, fluorides and phosphates (such as MgO, ZnO, $Al_2O_3$, $AlF_3$, $AlPO_4$, etc.) represents an effective way of controlling the electrochemical performance of commercially available $LiCoO_2$ electrodes by improving the structural integrity and by keeping down the electrode–electrolyte reaction [21–28]. Another approach to the improvement of the electrochemical performance of $LiCoO_2$ is simple re-annealing at temperatures up to 550 °C [29]. Recently, Tirado et al. demonstrated that rotor blade grinding followed by re-annealing affected strongly the microstructure, surface and morphology of $LiCoO_2$. As a result, a significant improvement in the electrochemical performance of $LiCoO_2$ was achieved [30,31]. Irrespective of the fact that many experimental techniques have been applied to understanding the physical meaning of the modified properties of $LiCoO_2$, they still remain unclear [32].

The electrochemical performance of $LiCoO_2$ is a complex process. One of the factors that is usually not taken into account, is the appearance of impurity ions in low concentration. Cobalt salts used for the production of $LiCoO_2$ contain usually impurities such as nickel and iron in concentrations less than 0.2%. In $LiCoO_2$, both $Ni^{3+}$ and $Fe^{3+}$ ions substitute for $Co^{3+}$ ions [7–10]. While $Ni^{3+}$ ions adopt low-spin configuration with S = 1/2, $Fe^{3+}$ ions are in high spin configuration with S = 5/2. One of the experimental methods especially suitable for studying transition metal ions at a low concentration level is the EPR spectroscopy working at 9.2 GHz (X-band EPR) [33–35]. Recently, enormous extending of the EPR capability as a local spectroscopic tool was achieved due to the application of a higher microwave frequency and a stronger magnetic field

* Corresponding autor at: Institute of General and Inorganic Chemistry, Bulgarian Academy of Sciences, Acad. G. Bonchev Str., bldg. 11, 1113 Sofia, Bulgaria. Tel.: +359 2 9793915; fax: +359 2 870 50 24.
*E-mail address:* radstoy@svr.igic.bas.bg (R. Stoyanova).

0378-7753/$ – see front matter © 2009 Elsevier B.V. All rights reserved.
doi:10.1016/j.jpowsour.2009.05.026

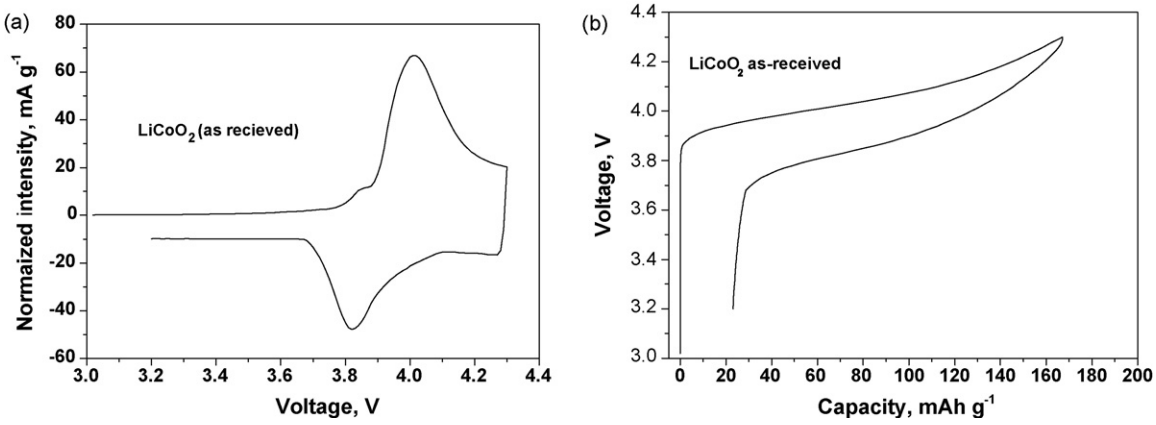


**Fig. 1.** SPES results corresponding to the first charge–discharge curve of bare $LiCoO_2$ in Li cells: (a) intensity vs. voltage curve and (b) voltage vs. capacity curve.

[36]. This technique is now recognized as high-frequency EPR working at frequencies and magnetic fields higher than 95 GHz and 3 T, respectively. For systems with S = 1/2, HF-EPR allows resolving small *g*-tensor anisotropy, while for systems with an integer spin or S > 1/2, the higher field used permits precise determination of the axial and rhombic zero field splitting (ZFS) parameters [36,37]. Concerning cathode materials for lithium ion batteries, the multi-frequency EPR spectroscopy provides an unique information on the local structure of $Ni^{3+}$ and $Fe^{3+}$ spin probes in $LiCoO_2$ and Al/Ga-substituted $LiCoO_2$, due to diamagnetic character of $Co^{3+}$ and $Al^{3+}/Ga^{3+}$ ions [38–40].

This study is aimed at analyzing the contribution of $Fe^{3+}$ and $Ni^{3+}$ impurities to the electrochemical performance of $LiCoO_2$ electrode materials. Commercial $LiCoO_2$ powders supplied by Aldrich were used for this study. The electrochemical performance of $LiCoO_2$ was modified by rotor blade grinding of $LiCoO_2$ followed by thermal treatment. Structural information on $Fe^{3+}$ and $Ni^{3+}$ impurities was obtained using both conventional X-band and high-frequency EPR spectroscopy. The assignment of the EPR signals was based on application of EPR standards such as $Ni^{3+}$ and $Fe^{3+}$ doped $LiCoO_2$.

## 2. Experimental

Commercial $LiCoO_2$ (Aldrich, Lot #20804PR) was used as starting material. According to specification sheet, the maximum metallic impurities determined from ICP trace metal analysis are 3000 ppm. The lithium cobalt oxide powder was dispersed in N-methyl pyrrolidone (NMP) and the resulting slurry was ground in an Ultra Tur-rax-T18 apparatus working at 10,000 rpm in air atmosphere. The high-speed rotating movement of the blades favoured the exfoliation process. NMP was removed by heating to 120 °C in air for several hours. Ground samples were obtained after milling for 20, 45, 60, 80, and 180 min periods. In addition, the starting $LiCoO_2$ material and selected ground samples were re-annealed at 500 and 850 °C in static air atmosphere for 48 h inside an alumina crucible. Heating and cooling rates were ca. 2 $min^{-1}$. Selected samples were washed with acetone under magnetic stirring for 5 and 10 h and an additional heat treatment at 850 °C was carried out.

EPR measurements at 9.23 GHz were carried out in a ERS 220/Q spectrometer within the temperature range 85–410 K. The *g*-factors were established with respect to a $Mn^{2+}$/ZnS standard. The high-frequency EPR spectra were recorded on a single-pass transmission EPR spectrometer built in the High-Magnetic Filed Laboratory, Grenoble, France. The frequencies were changed from 95 to 345 GHz using Gunn diodes and their multipliers. The detection of absorption was performed with an bolometer. The recording temperatures were varied from 5 to 300 K using a variable temperature insert (Oxford Instruments). Simulation software SIM written by Weihe was used to extract numerical values of spin Hamiltonian parameters from experimental EPR spectra [41,42]. The program was based on a full-matrix diagonalization procedure and allowed generating powder pattern EPR spectra of spin systems with any values of zero-filed splitting parameters relative to the operating frequencies. This program also took into account the Boltzman population factor in calculating the EPR intensities.

Due to the lower sensitivity of the HF-EPR technique (single-pass technique) as compared to the conventional X-band EPR spectrometer, a higher spin concentration was needed. That is why the $LiCoO_2$ oxides were additionally doped with Ni and Fe in a concentration of Ni(Fe)/[Co + Ni(Fe)] = 0.005. In this case, the signal in the X-band EPR spectrum was broadened, but the EPR profile were preserved (not shown). Moreover, the crystal structure parameters of Ni- and Fe-doped $LiCoO_2$ oxides remained the same. The synthesis procedure was based on the co-precipitated hydroxide method, which is described in details elsewhere [43]. The solid-state reaction between Fe/Ni-doped cobalt hydroxide precursor with LiOH proceeds at 900 °C for 12 h in air. Both Ni- and Fe-doped $LiCoO_2$ were used as EPR standards for $Ni^{3+}$ and $Fe^{3+}$ ions.

In order to obtain the electrodes for the electrochemical experiments, the $LiCoO_2$ active material (77%) was mixed with PVDF (8%) and graphite (15%), and dispersed in NMP. After heating to 150 °C in vacuum for several hours, the resulting composite electrodes were supported on Al-foil and used as positive electrodes in lithium cells. The electrochemical behaviour of $LiCoO_2$-based positive electrodes was studied in lithium cells. In the Swageloke-type cells, the negative electrode consisted of a clean 9 mm diameter lithium metal disk. The commercial (Merck LP40) electrolyte solution was 1 M LiPF6 in a 1:1 mixture of ethylene carbonate (EC) and diethyl carbonate (DEC), which was supported in Whatman™ glass microfibers as separators. Step Potential Electrochemical Spectroscopy (SPES) experiments were carried out with a MacPile-II instrument, by applying potential steps of 10 mV every 0.1 h in the range between 4.3 and 3.2 V.

## 3. Results and discussion

### 3.1. Electrochemistry and EPR spectrum of bare $LiCoO_2$

Fig. 1 gives the SPES curves of commercial $LiCoO_2$. The SPES curves show the typical electrochemical behavior of well-known $LiCoO_2$: the main oxidation peak is observed at ca. 4.1 V, and the main reduction peak at ca. 3.82 V. These effects correspond to the redox couple $Co^{3+}/Co^{4+}$ and are accompanied by a significant expansion of the *c* parameter during lithium extraction

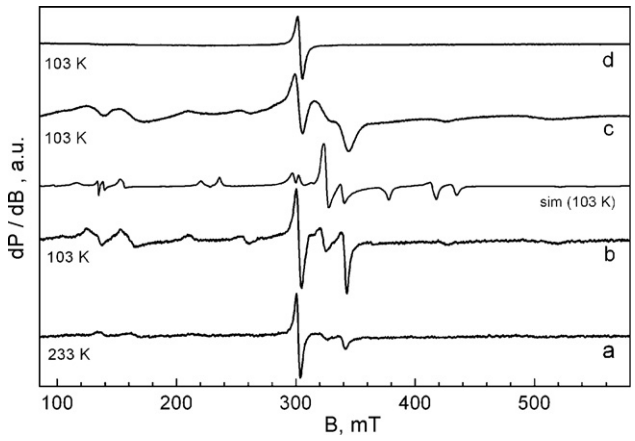


**Fig. 2.** X-band EPR spectra at 233 K (a) and 103 K (b) of bare $LiCoO_2$. For the signal assignment, the EPR spectra at 103 K of $LiCoO_2$ doped with Fe (c) and Ni (d) are also shown. The simulated EPR spectrum at 9.2 GHz (sim(103 K)) for $Fe^{3+}$ with $g_1 = 1.9908$, $g_2 = 1.9922$, $g_3 = 2.0033$ and $D = 0.0545\ cm^{-1}$, $E/D = 0.262$ is also given.

[44]. However, the two small peaks commonly observed at higher voltage ascribable to an order–disorder transition of $Li^+$ ions in the interlayer are not clearly observable [45]. Previous studies on this material showed that the two low-intensity peaks were only observable in highly crystalline $LiCoO_2$ samples [30]. The voltage–capacity curve shows that the reversible capacity measured in the first cycle is 144 mAh $g^{-1}$ (Fig. 1b).

$Co^{3+}$ ions, which adopt the low-spin configuration in $LiCoO_2$, are diamagnetic. This means that $LiCoO_2$ is not active in EPR experiments. However, well-resolved EPR spectrum in the X-region is observed for bare $LiCoO_2$ (Fig. 2). To facilitate the assignment of EPR signals, the same figure gives the EPR spectra of low-spin $Ni^{3+}$ and $Fe^{3+}$ ions stabilized in $LiCoO_2$ in concentration level of 0.5%. Comparison of the EPR spectra of bare $LiCoO_2$ and EPR standards allows differentiating between two types of signals. At 233 K, the single line with Lorentzian shape and *g*-factor of 2.142 dominates in the EPR spectrum of bare $LiCoO_2$. This signal is attributed to low-spin $Ni^{3+}$ ions. On cooling, the second type of signal becomes visible. This EPR signal consists of multiple lines that are spanned over a wide field range. Based on our previous EPR studies of $Fe^{3+}$ in $LiAl_yCo_{1-y}O_2$ oxides [40], the structured EPR patterns come from $Fe^{3+}$ ions, for which the magnitude of the ZFS parameter is comparable with the energy of the microwave frequency ($h\nu \approx 0.3\ cm^{-1}$, low field approximation).

EPR spectroscopy at high frequencies provides further information on the local coordination of $Ni^{3+}$ and $Fe^{3+}$ impurity ions in $LiCoO_2$. Fig. 3 gives the HF-EPR spectra of bare $LiCoO_2$ and EPR standards for $Fe^{3+}$ and low-spin $Ni^{3+}$ ions. Between 100 and 30 K, two well separated signals due to low-spin $Ni^{3+}$ and $Fe^{3+}$ ions give rise to the EPR spectrum of bare $LiCoO_2$ registered at 285 GHz: a single Lorentzian line with $g = 2.142$ and a signal with tetragonal symmetry with $g_\perp = 1.9921$ and $g_{||} = 2.0027$, respectively. In this temperature range the tetragonal signal dominates. As $Ni^{3+}$ is an ion with S = 1/2, the *g*-value remains the same when is determined at lower and higher frequencies. As $Fe^{3+}$ is an ion with S = 5/2, the EPR spectrum is more complex due to the splitting of the six magnetic sublevels of the ground spin state in zero-magnetic field. In addition to the central anisotropic signal, several weaker signals symmetrically shifted to down- and upper-field become visible. Their intensities increase on cooling. At 5 K, two intensive outermost signals at 10.0 and 10.4 T dominate the EPR spectrum. The temperature dependence of the line position and line intensity permit determination of the axial and rhombic ZFS parameters for $Fe^{3+}$ ions in $LiCoO_2$. The details of this procedure have been described elsewhere [40]. Thus, the values of axial and rhombic ZFS parameters are as follows: $D = 0.0545\ cm^{-1}$ and $E/D = 0.262$. To check the correctness of ZFS determination, Figs. 2 and 3 give also the simulated EPR spectrum at 9.2 and 95 GHz. The same values of ZFS parameters have been determined for $Fe^{3+}$ in Fe-doped $LiCoO_2$ [40]. This means that the magnitude of ZFS parameters does not depend on the amount of $Fe^{3+}$ ions.

By modeling of the magnitude of ZFS parameters in the framework of the Newman superposition model [40], it has been found that $Fe^{3+}$ ions occupy sites in the Co-layers characterized by a lower extent of trigonal distortion, but by an increased rhombic deformation. However, for the host matrices, trigonally distorted sites are only available. The appearance of local rhombic distortion around $Fe^{3+}$ ions does not affect the massive trigonal distortion of $CoO_2$-layers. The appearance of $Fe^{3+}$ in distorted crystal field has also been detected by $^{57}Fe$ Mössbauer spectroscopy [46–49]. After partial replacement of $Co^{3+}$ by $Fe^{3+}$ ($0 < x < 0.2$), $Fe^{3+}$ ions having a smaller isomer shift (0.24–0.19 mm $s^{-1}$) appear. These ions have been assigned to $Fe^{3+}$ ions located in pseudotetrahedral sites in $LiO_2$-layers or in square-pyramidal sites (in $CoO_2$-layers) formed with the participation of an oxygen vacancy [48,49].

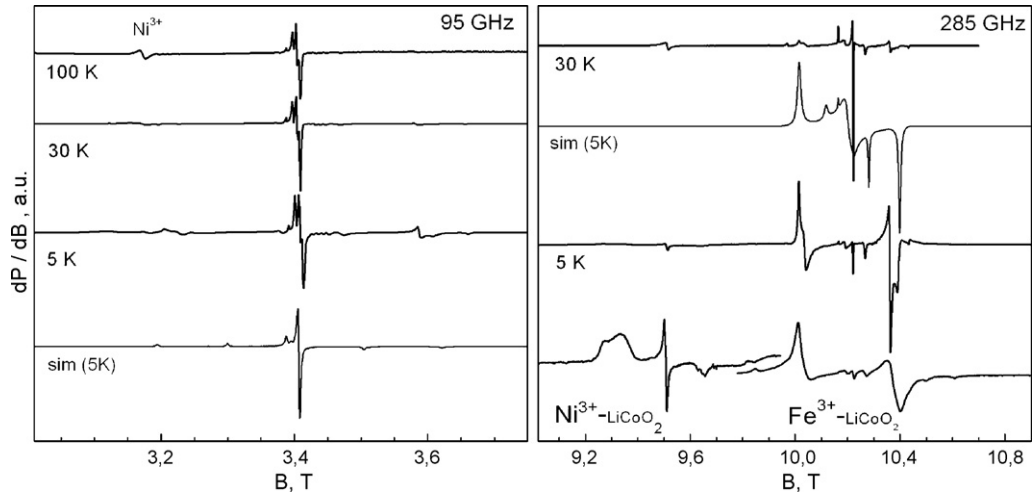


**Fig. 3.** EPR spectra at 95 and 285 GHz of bare $LiCoO_2$. The operating temperature is 5 K, 30 K and 100 K for 95 GHz experiments and 5 and 30 K for 285 GHz, respectively. For the signal assignment, the EPR spectra at 285 GHz of $LiCoO_2$ doped with $Fe^{3+}$ and $Ni^{3+}$ are shown ($Ni^{3+}$–$LiCoO_2$ and $Fe^{3+}$–$LiCoO_2$, respectively). Simulated EPR spectra at 95 and 285 GHz (5 K operating temperature) for $Fe^{3+}$ with $g_1 = 1.9908$, $g_2 = 1.9922$, $g_3 = 2.0033$ and $D = 0.0545\ cm^{-1}$, $E/D = 0.262$ are also given (sim(5 K)).

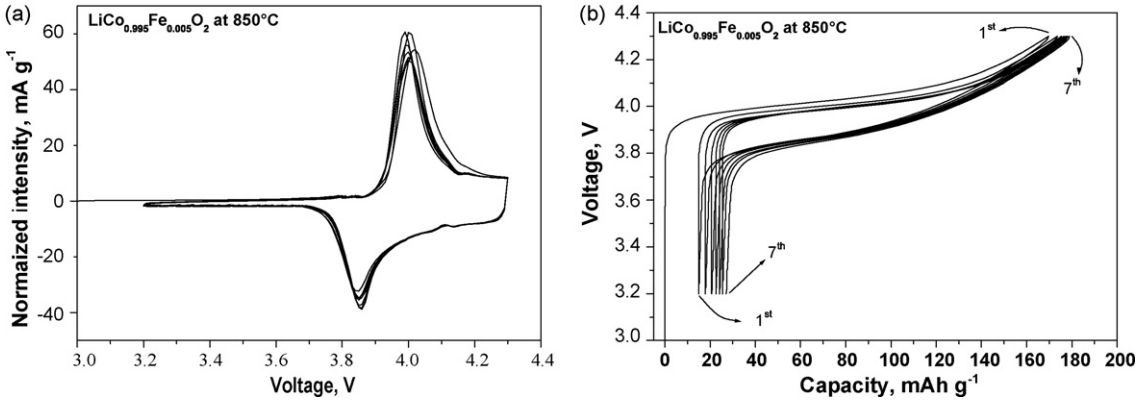


**Fig. 4.** SPES results corresponding to the seven first charge–discharge cycles of $LiCo_{0.995}Fe_{0.005}O_2$ synthesised by co-precipitated method at 850 °C in Li cells: (a) intensity vs. voltage curve and (b) voltage vs. capacity curve.

At 5 K, the isotropic signal due to $Ni^{3+}$ is split into anisotropic doublet and a nearly symmetric single line in the central part (Fig. 3). According to our previous EPR studies on $Ni^{3+}$ doped $LiAl_yCo_{1-y}O_2$ [50,51,38,39], the anisotropic doublets originate from the ground vibronic doublet state, while the single line can be assigned to an excited vibronic singlet and/or relaxation averaged singlet. This means, that contrary to $Fe^{3+}$ ions, $Ni^{3+}$ ions occupy the trigonally distorted sites in the Co-layers, where the orbitally degenerate state for $Ni^{3+}$ is preserved.

For a concentration of 0.5%, the insertion of $Fe^{3+}$ ions in $LiCoO_2$ does not significantly affect the value of reversible capacity in the first cycle: 155 mAh $g^{-1}$ (Fig. 4). Close inspection of SPES curves shows that $Fe^{3+}$ impurities suppress the order–disorder transition of $Li^+$ ions. The effect of impurity ions on this process has been reported by Dahn et al. [45].

### 3.2. Effect of grinding on the EPR spectrum and electrochemical performance of $LiCoO_2$

Detection of $Fe^{3+}$ and $Ni^{3+}$ impurities allows us to use these two ions as EPR probes in order to follow the local structural changes caused by grinding of $LiCoO_2$. According to our previous studies, three features of the grinding process can be outlined [30]: (i) short grinding times (20 min) lead to the formation of exfoliated layers inside larger particles; (ii) medium grinding times (60–120 min) give rise to ultrafine layered particles, and (iii) on prolonged grinding (80–180 min), lithium cobalt oxide reacts with the atmosphere resulting in the formation of a thick lithium carbonate surface film. Based on X-ray absorption spectroscopic study [31], it has been found that the layered structure (in terms of Co–Co and Co–O distances) is basically preserved after mechanical and thermal treatment. However, after grinding the electrochemical performance of $LiCoO_2$ undergoes a significant change: a poor electrochemical behaviour was observed after short and prolonged grinding times (up to 20 min and above 80 min, respectively), while, with an intermediate grinding time (about 60 min), there is a net improvement in the reversible specific capacity and capacity retention [30]. To eliminate the effect of $Li_2CO_3$ deposition on the surface of $LiCoO_2$ particles ground for 180 min, the sample was additionally washed with acetone for 5 and 10 h. SPES curves of ground and ground-washed $LiCoO_2$ samples are compared in Fig. 5. As one can see, after washing there are two important remarkable differences in the electrochemical behaviour: (i) the cathodic and anodic peaks are less broadened and more intense as compared with the un-washed sample (Fig. 5a) and (ii) there is an improvement of the reversible capacity in the first cycle. The capacity value is increased from 63 to 115 mAh $g^{-1}$ (Fig. 5b), but this behavior is still worse as compared to untreated $LiCoO_2$ (Fig. 1). However, the capacity retention is enhanced on cycling as can be discussed later in terms of cycling stability.

To get insight into the effect of the grinding process, EPR as a local spectroscopic technique is invoked. Fig. 6 gives the EPR spectra of bare and treated $LiCoO_2$. After grinding, the EPR spectrum of $LiCoO_2$ undergoes a strong change. A short grinding time (up to 20 min) leads to a decrease in intensity of the signal due to $Fe^{3+}$ ions. In the same sequence, it appears that the signal due to $Ni^{3+}$ remains unchanged. In addition, a new signal grows in intensity. This signal is significantly broadened as compared to the signal due to isolated $Ni^{3+}$ and $Fe^{3+}$ impurity ions. In addition, the resonance

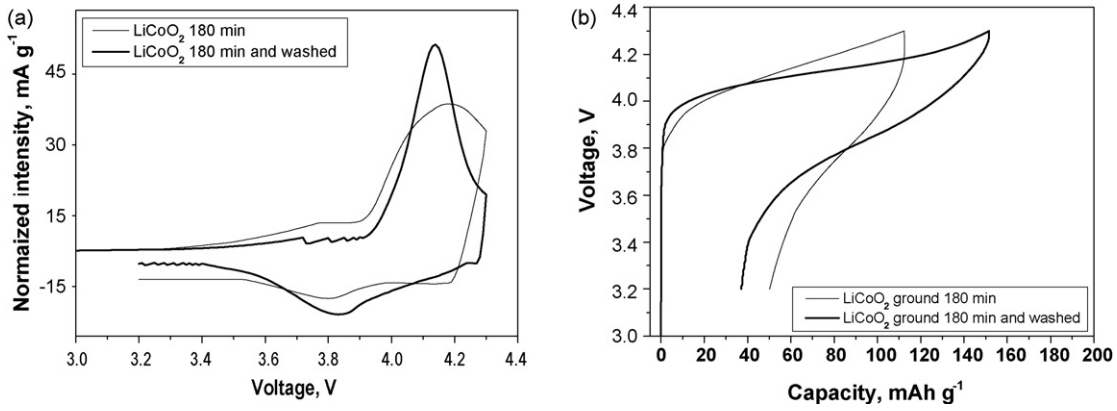


**Fig. 5.** SPES results corresponding to the first charge–discharge curve of $LiCoO_2$ ground 180 min and $LiCoO_2$ ground 180 min and washed with acetone for 10 h, in Li cells. (a) Intensity vs. voltage curve and (b) voltage vs. capacity curve.

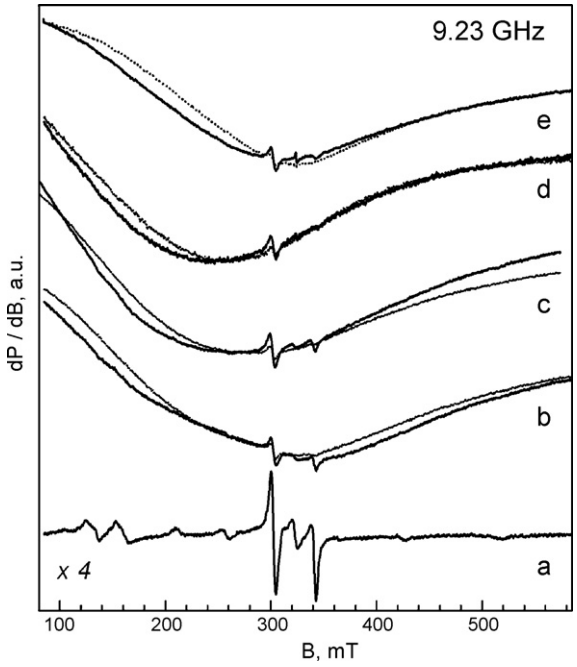


**Fig. 6.** X-band EPR spectra of: bare $LiCoO_2$ (a); $LiCoO_2$ after grinding for 20 min; (b) 60 min (c); and 180 min (d), and ground $LiCoO_2$ for 180 min followed by washing with acetone for 10 h (e). Dotted and full lines correspond to the EPR spectra registered at 293 K and 103 K, respectively. The intensity scale of bare $LiCoO_2$ is magnified 4 times as compared to that of other samples.

absorption depends on the operating temperature. On cooling from 293 to 103 K, the magnetic resonance is shifted to a lower magnetic field, which corresponds to the change in the effective *g*-factor from 3.8 to 4.0. After further grinding, there is a continuous shift of the resonance absorption towards the lower magnetic fields: the effective *g*-value increases from about 4.0 to about 5.0 for samples ground for 20 and 180 min. For oxide treated for 180 min, the signal

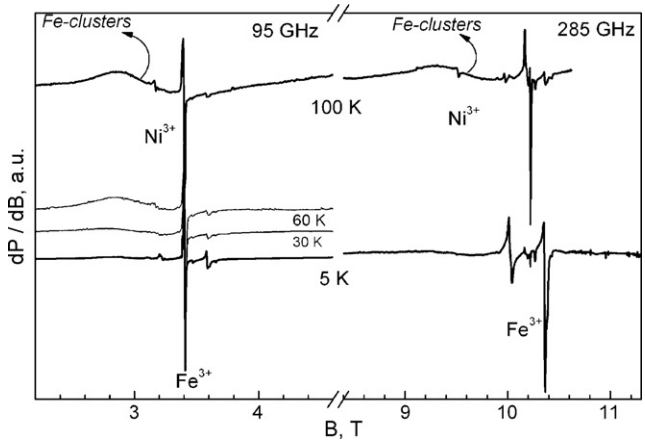


**Fig. 7.** HF-EPR spectra of $LiCoO_2$ ground for 60 min.

due to $Fe^{3+}$ ions is poorly visible at the expense of the broad signal (Fig. 6). It is worth mentioning that the broader signal is affected after the washing of ground $LiCoO_2$. There are a line broadening and a shift of magnetic resonance to a higher field (Fig. 6d and e). In the same sequence, the effective *g*-factor decreases from 5.0 to 3.3.

The EPR parameters permit assigning the broad signal to metal clusters rather than to isolated paramagnetic centers. To support this suggestion, Fig. 7 gives the HF-EPR spectra of $LiCoO_2$ ground for 60 min. At 100 K, the HF-EPR spectra consist of a broad signal with a *g*-value decreasing with increasing microwave frequency and reaching the *g*-value of free electron at 285 GHz: *g*-values of 4.68, 2.22 and 2.10 for the microwave frequency of 9.2, 95 and 285 GHz, respectively. The line width determined at 95 and 285 GHz remains constant: 0.55 T. This signal is broadened on cooling and disappears below 30 K. The observed EPR parameters can be related to the formation of metal clusters, where metal ions are coupled by weak antiferromagnetic interactions. The approach of the effective *g*-values to the *g*-factor of the free electron indicates that $Fe^{3+}$

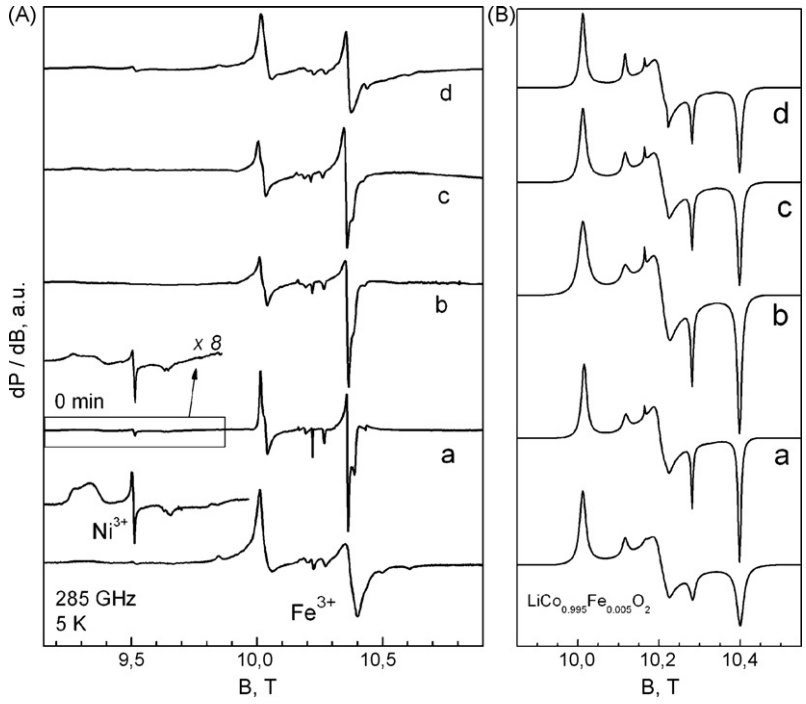


**Fig. 8.** (A) EPR spectra at 285 GHz of bare $LiCoO_2$ (a) and $LiCoO_2$ ground for 60 min (b) and re-annealed at 500 °C (c) and 850 °C (d). For the signal assignment, the EPR spectra of $Ni^{3+}$ and $Fe^{3+}$ ions in Ni and Fe-doped $LiCoO_2$ are also shown. (B) Simulated EPR spectra (sim(5 K)) including *D*-strain broadening are also given.

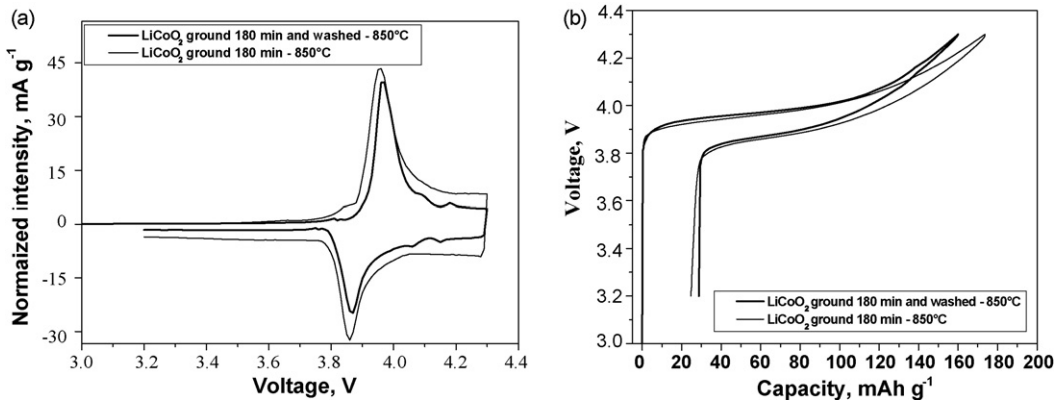


**Fig. 9.** SPES results corresponding to the first charge–discharge curve of $LiCoO_2$ ground 180 min, and $LiCoO_2$ ground 180 min followed of washing 10 h and then reheated at 850 °C, in Li cells (a) intensity vs. voltage curve and (b) voltage vs. capacity curve.

ions are mainly involved in the cluster formation. The formation of Fe(III)–O clusters with predominate antiferromagnetic interactions has been established by Scholz et al. after ball milling of nanostructured $Al_2O_3$ [52]. It is noticeable that iron clusters start to form after short milling time of $Al_2O_3$ (about 5 min.).

Another feature of the HF-EPR spectra of treated $LiCoO_2$ is the signal due to isolated $Fe^{3+}$ ions. Fig. 8 compares the HF-EPR spectra of bare $LiCoO_2$, treated $LiCoO_2$ and Fe-doped $LiCoO_2$ in the region where the $Fe^{3+}$ signal is well resolved. At 5 K, all samples studied displays two intensive outermost signals at 10.0 and 10.4 T due to $|\pm5/2> - |\pm3/2>$ multiplet transition. By increasing the operating temperature, the central asymmetric signal due to $|-1/2> - |+1/2>$ transition grows in intensity. The identical line positions and close temperature dependence of the line intensities indicate clearly the same magnitude of ZFS parameters for bare and treated $LiCoO_2$, as well as for $Fe^{3+}$-doped $LiCoO_2$.

Contrary to the $Fe^{3+}$ signal, the signal due to low-spin $Ni^{3+}$ ions remains unaffected after grinding. This means that grinding of $LiCoO_2$ affects the cationic distribution of $Fe^{3+}$ impurity ions only. This finding is consistent with local distortion of the $Fe^{3+}$ and $Ni^{3+}$ site in $LiCoO_2$. The short-time grinding provokes an extraction of $Fe^{3+}$ ions from Co-position, this leading to their segregation into $Fe^{3+}$-clusters. After further grinding, there is a continuous redistribution of $Fe^{3+}$, as a result of which the axial stresses are accommodated in the layers. The formation of Fe clusters has a negative effect on the electrochemical performance of $LiCoO_2$, while isolated $Fe^{3+}$ impurities act beneficially.

### 3.3. *Effect of re-annealing on the EPR spectrum and electrochemical performance of $LiCoO_2$*

The re-annealing of ground $LiCoO_2$ has been shown to promote its electrochemical behaviour [30]. Based on XPS studies, the performance improvement is a result of the elimination of surface lithium carbonate by thermal treatment due to lithium and oxygen reincorporation into $LiCoO_2$. This process proceeds only after re-annealing of $LiCoO_2$ at 850 °C, while the particle surface remains unchanged after re-annealing at 500 °C. The re-annealing is an effective process even in the case when ground $LiCoO_2$ is washed (Fig. 9). For this oxide, the SPES curves display well-resolved peaks due to oxidation/reduction of Co ions and to the order/disorder of $Li^+$ ions. In comparison with unwashed oxide, the capacity remains slightly lower (Fig. 9b). This is related to partial dissolving of surface lithium carbonate deposed after prolonged grinding.

A cycling life study of the electrodes was carried out (Fig. 10). Iron doped samples $LiCo_{0.995}Fe_{0.005}O_2$ containing isolated $Fe^{3+}$ ions exhibit a high reversible capacity. The maximum reversible capacity was 155 mAh $g^{-1}$ and after 50 cycles 135 mAh $g^{-1}$ leading to an efficiency of 87%. A similar capacity value during the first few cycles was observed for the sample which was previously ground (180 min), washed and afterwards re-annealed at 850 °C, being the only difference in a lower efficiency (82%). An improvement in the reversible capacity value of ground and washed $LiCoO_2$ sample as compared with an un-washed sample [30] was observed, but the capacity faded drastically after 12 cycles. It is demonstrated by electrochemical means that all these re-annealed samples recover their characteristic reversible capacity not only in the first cycles but also on prolonged cycling.

The temperature where samples are re-annealed has a direct effect on Fe re-distribution. Fig. 11 gives the EPR spectra of $LiCoO_2$ ground for 60 min and re-annealed at 500 and 850 °C. When samples are re-annealed at 500 °C, the broad signal still remains. However, the EPR parameters are changed: the line width decreases and the resonance absorption is shifted to higher magnetic field. The line shape depends on the operating temperature: the symmetric narrow line is strongly broadened on cooling. The observed changes in the EPR parameters of the broad signal reveal a reorganization of the Fe-clusters after re-annealing of $LiCoO_2$ at 500 °C. By increasing the re-annealing temperature from 500 to 850 °C, a broad signal due to iron clusters disappears. In the same sequence, there is a recovering of the EPR signals due to isolated $Fe^{3+}$ ions. This feature does not depend on the grinding time. Fig. 11 compares the EPR spectra of $LiCoO_2$ ground for a short- and a prolonged time fol-

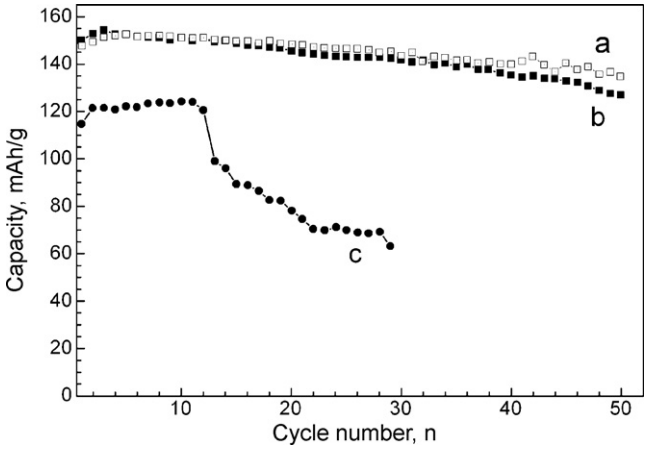


**Fig. 10.** Cycling performance of the electrodes: (a) $LiCo_{0.995}Fe_{0.005}O_2$; (b) $LiCoO_2$ ground for 180 min, washed with acetone and re-annealed at 850 °C; (c) $LiCoO_2$ ground for 180 min.

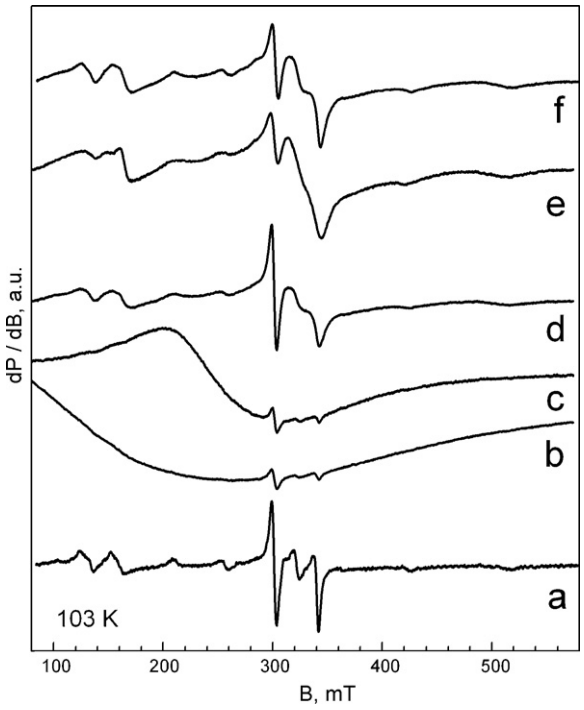


**Fig. 11.** X-band EPR spectra of: bare $LiCoO_2$ (a); $LiCoO_2$ ground for 60 min (b); $LiCoO_2$ ground for 60 min and re-annealed at 500 °C (c); $LiCoO_2$ ground for 60 min and re-annealed at 850 °C (d); $LiCoO_2$ ground for 180 min and re-annealing at 850 °C (e); $LiCoO_2$ ground for 180 min, washed with acetone for 10 h and re-annealing at 850 °C (f).

lowed by re-annealing at 850 °C. Irrespective of the grinding time, the broad signal disappears after re-annealing. The disappearance of the broad signal is concomitant with recovering of the signal due to isolated $Fe^{3+}$ ions.

The re-annealing process affects also the isolated $Fe^{3+}$ ions. Close inspection of the HF-EPR spectra of ground and re-annealed oxides (Fig. 8) shows that the intensities of two outermost signals at 10.0 and 10.4 T are different. The ground $LiCoO_2$ displays an increased intensity ratio of the two multiplet signals, while there is a smooth decrease after re-annealing of $LiCoO_2$ at 500 and 850 °C. This feature can be related to the contribution of *D*-strain broadening to the EPR profile. The higher is the *D*-strain broadening, the higher is the difference between the intensities of two signals. Fig. 8 gives the simulated EPR spectra of bare $LiCoO_2$, ground $LiCoO_2$ and re-annealed $LiCoO_2$ at 500 and 850 °C by using *D*-strain broadening as follows: 0.0015, 0.0020, 0.0011 and 0.0004, respectively. The important finding is that the grinding of $LiCoO_2$ induces strains around isolated $Fe^{3+}$ ions, which are cured after re-annealing of $LiCoO_2$ at 850 °C.

The EPR studies demonstrate that iron distribution in $LiCoO_2$ is a sensitive towards both mechanical and thermal treatments, while $Ni^{3+}$ remains intact. This allows associating the iron re-distribution process with observed changes in the electrochemical performance of $LiCoO_2$ (Figs. 5 and 10). The improvement of the electrochemical performance of $LiCoO_2$ is associated with the disappearance of iron clusters, as well as with the annihilation of strains around isolated $Fe^{3+}$ ions. This means that the iron clusters displays a tendency to block lithium diffusion, resulting in a worse electrochemical behavior of $LiCoO_2$. It should be noted that the ionic radius of the $Fe^{3+}$ ion is significantly larger than that of the $Co^{3+}$ ions, thus resulting in a pinning of the interlayers by the iron clustering process (Scheme 1). Contrary to iron clustering, the ionic mismatch causes a local rhombic distortion around isolated $Fe^{3+}$ ions in trigonal layers, which does not disturb the lithium diffusion.

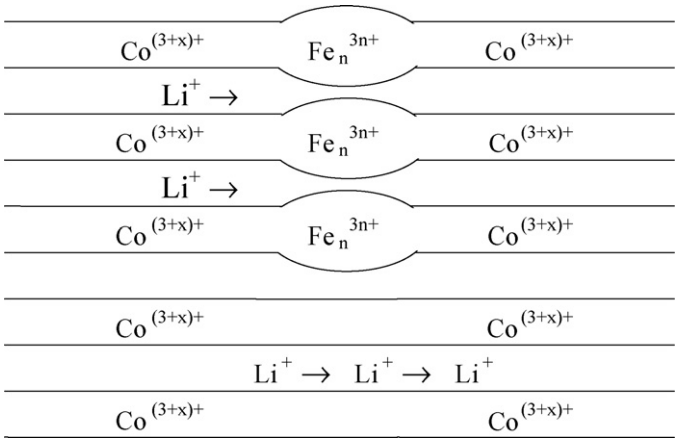


**Scheme 1.** Schematic blocking mechanism of iron clusters on lithium diffusion.

## 4. Conclusion

Commercial $LiCoO_2$ powders supplied by Aldrich contain isolated $Fe^{3+}$ and $Ni^{3+}$ impurity ions, which occupy the $Co^{3+}$-sites in $CoO_2$-layers. The accommodation of $Fe^{3+}$ in $CoO_2$-layers creates a local rhombic distortion, while trigonal distorted site is preserved after appearance of $Ni^{3+}$. This feature is not unique for commercial $LiCoO_2$. It is a consequence of impurities contamination of the initial cobalt salts used for production of $LiCoO_2$. The appearance of $Fe^{3+}$ and $Ni^{3+}$ impurities contribute also to the electrochemical properties of $LiCoO_2$.

Iron-bearing $LiCoO_2$ was modified by rotor blade grinding, which led to three main effects: (i) particle comminution by exfoliation, (ii) surface deposition of a lithium carbonate layer, and (iii) iron clustering. These effects resulted in the poorer electrochemical behavior of lithium test cells. The particle surface can be cleaned by acetone washing, which yields partial improvement in the electrode performance. Re-annealing improves crystallinity and destroys the iron clusters, which leads to a net improvement in the electrochemical properties. The results can be interpreted in terms of a blocking effect in lithium diffusion caused by the iron clusters. This effect is also evidenced by the difficulty in lithium ordering, as revealed by the high-voltage order–disorder transition effects in the electrochemical spectroscopy curves.

## Acknowledgements

Authors are indebted to the National Science Fund of Bulgaria (contract no. Ch1701/2007) for financial support. The high-frequency EPR measurements carried out at High Magnetic Field Laboratory in Grenoble, France, were supported by the European Commission within the 6th framework programme "Transnational Access – Specific Support Action" (contract no. RITA-CT-2003-505474) – "Access to research in very high magnetic field". RA, GO and JLT are grateful to CICYT (MAT2008-05880) and Junta de Andalucía (FQM-1447) for financial support. EZ, RS and SI acknowledge the financial support by the National Science Fund of Bulgaria (National Centre for New Materials UNION, contract no. DO-02-82/2008).

## References

[1] M.S. Whittingham, Chem. Rev. 104 (2004) 4271–4301.
[2] H.J. Orman, P.J. Wiseman, Acta Cryst. C 40 (1984) 12–14.
[3] J.B. Goodenough, J. Power Sources 174 (2007) 996–1000.
[4] T. Ohzuku, A. Ueda, M. Nagayama, Y. Iwakoshi, H. Komori, Electrochim. Acta 38 (1993) 1159–1167.
[5] I. Nakai, K. Takahashi, Y. Shiraishi, T. Nakagome, F. Izumi, Y. Ishii, F. Nishikawa, T. Konishi, J. Power Sources 68 (1997) 536–539.

[6] I. Nakai, K. Takahashi, Y. Shiraishi, T. Nakagome, F. Izumi, Y. Ishii, F. Nishikawa, T. Konishi, J. Electrochem. Soc. 151 (2004) A672–A681.
[7] C. Delmas, I. Saadoune, Solid State Ionics 53–56 (1992) 370–375.
[8] E. Zhecheva, R. Stoyanova, Solid State Ionics 66 (1993) 143–149.
[9] M. Holzapfel, R. Schreiner, A. Ott, Electrochim. Acta 46 (2001) 1063–1070.
[10] R. Alcántara, P. Lavela, C.P. Vicente, J.L. Tirado, J. Olivier-Fourcade, J.C. Jumas, Solid State Commun. 115 (2000) 1–6.
[11] R. Stoyanova, E. Zhecheva, L. Zarkova, Solid State Ionics 73 (1994) 233–240.
[12] A.R. Armstrong, A.D. Robertson, R. Gitzendanner, P.G. Bruce, J. Solid State Chem. 145 (1999) 549–556.
[13] G. Ceder, Y.-M. Chiang, D.R. Sadoway, M.K. Aydinol, Y.-I. Jang, B. Huang, Nature 392 (1998) 694.
[14] R. Alcántara, P. Lavela, R.L. Relano, J.-L. Tirado, E. Zhecheva, R. Stoyanova, Inorg. Chem. 37 (1998) 264–269.
[15] R. Stoyanova, E. Zhecheva, G. Bromiley, T. Boffa Ballaran, R. Alcántara, J.I. Corredor, J.L. Tirado, J. Mater. Chem. 12 (2002) 2501–2506.
[16] H. Tukamoto, A.R. West, J. Electrochem. Soc. 144 (1997) 3164–3168.
[17] M. Mladenov, R. Stoyanova, E. Zhecheva, S. Vassilev, Electrochem. Commun. 3 (2001) 410–416.
[18] S. Gopukumar, Y. Jeong, K.B. Kim, Solid State Ionics 159 (2003) 223–232.
[19] S. Levasseur, M. Menetrier, Y. Shao-Horn, L. Gautier, A. Audemer, G. Demazeau, A. Largeteau, C. Delmas, Chem. Mater. 15 (2003) 348–354.
[20] M. Menetrier, D. Carlier, M. Blangero, C. Delmas, Electrochem. Solid State Lett. 11 (2008) A179–A182.
[21] H.-J. Kweon, D.G. Park, Electrochem. Solid State Lett. 3 (2000) 128–130.
[22] J. Cho, Y.J. Kim, B. Park, Chem. Mater. 12 (2000) 3788–3791.
[23] E. Zhecheva, M. Mladenov, R. Stoyanova, S. Vassilev, J. Power Sources 162 (2006) 823–828.
[24] A. Choblet, H.C. Shiao, H.-P. Lin, M. Salomon, V. Manivannan, Electrochem. Solid State Lett. 4 (2001) A65–A67.
[25] Zh. Wang, Ch. Wu, L. Liu, F. Wu, L. Chen, X. Huang, J. Electrochem. Soc. 149 (2002) A466–A471.
[26] L. Liu, L. Chen, X. Huang, X.-Q. Yang, W.-S. Yoon, H.S. Lee, J. McBreen, J. Electrochem. Soc. 151 (2004) A1344–A1351.
[27] D. Ahn, C. Kim, J.-G. Lee, B. Kim, Y. Park, B. Park, J. Mater. Res. 22 (2007) 688.
[28] Y. Kim, Y. Hong, K.S. Ryu, M.G. Kim, J. Cho, J. Power Sources 179 (2008) 780–784.
[29] Zh. Chen, J.R. Dahn, Electrochem. Solid State Lett. 7 (2004) A11–A14.
[30] R. Alcántara, G.F. Ortiz, P. Lavela, J.L. Tirado, W. Jaegermann, A. Thissen, J. Electroanal. Chem. 584 (2005) 147–156.
[31] A.V. Chadwick, S.L.P. Savin, R. Alcántara, D.F. Lisbona, P. Lavela, G.F. Ortiz, J.L. Tirado, ChemPhysChem 7 (2006) 1086–1091.
[32] N. Pereira, J.F. Al-Sharab, F. Cosandey, F. Badway, G.G. Amatucci, J. Electrochem. Soc. 155 (2008) A831–A838.
[33] D.J. Keeble, M. Loyo-Menoy, Y. Furukawa, K. Kitamura, Phys. Rev. B 71 (2005) 224111.
[34] H. Meštrić, R.-A. Eichel, T. Kloss, K.-P. Dinse, So. Laubach, St. Laubach, P.C. Schmidt, K.A. Schönau, M. Knapp, H. Ehrenberg, Phys. Rev. B 71 (2005) 134109.
[35] H. Meštrić, R.-A. Eichel, K.-P. Dinse, A. Ozarowski, J. van Tol, L.C. Brunel, H. Kungl, M.J. Hoffmann, K.A. Schönau, M. Knapp, H. Fuess, Phys. Rev. B 73 (2006) 184105.
[36] J. Krzystek, A. Ozarowski, J. Tesler, Coord. Chem. Rev. 250 (2006) 2308–2324.
[37] K.K. Anderson, A.-L. Barra, Spectrochim. Acta A 58 (2002) 1101.
[38] R. Stoyanova, E. Zhecheva, R. Alcántara, J.L. Tirado, J. Phys. Chem. B 108 (2004) 4053–4057.
[39] E. Zhecheva, R. Stoyanova, R. Alcántara, J.L. Tirado, J. Phys. Chem. B 107 (2003) 4290–4295.
[40] R. Stoyanova, A.-L. Barra, E. Zhecheva, R. Alcántara, G. Ortiz, J.-L. Tirado, Inorg. Chem. 48 (2009) 4798–4805.
[41] J. Glerup, H. Weihe, Acta Chem. Scand. 45 (1991) 444.
[42] SIM software by Høgni Weihe, Institute of Chemistry, University of Copenhagen, Denmark.
[43] (a) M. Yoncheva, R. Stoyanova, E. Zhecheva, R. Alcántara, G. Ortiz, J.L. Tirado, Electrochim. Acta 54 (2009) 1694–1701;
(b) E. Shinova, R. Stoyanova, E. Zhecheva, G. Ortiz, P. Lavela, J.L. Tirado, Solid State Ionics 179 (2008) 2198–2208;
(c) M. Yoncheva, R. Stoyanova, E. Zhecheva, R. Alcaĭntara, J.L. Tirado, J. Alloys Comp. 475 (2009) 96–101.
[44] J.N. Reimers, J.R. Dahn, J. Electrochem. Soc. 139 (1992) 2091–2097.
[45] J.N. Reimers, J.R. Dahn, U. von Sacken, J. Electrochem. Soc. 140 (1993) 2752–2754.
[46] R. Alcántara, J.C. Jumas, P. Lavela, J. Olivier-Fourcade, C. Pérez-Vicente, J.L. Tirado, J. Power Sources 81–82 (1999) 547–553.
[47] M. Tabuchi, K. Ado, H. Kobayashi, H. Sakaebe, H. Kageyama, C. Masquelier, M. Yonemura, A. Hirano, R. Kanno, J. Mater. Chem. 9 (1999) 199–204.
[48] L. Aldon, J. Olivier-Fourcade, J.-C. Jumas, M. Holzapfel, C. Darie, P. Strobel, J. Power Sources 146 (2005) 259–263.
[49] M. Ménétrier, Y. Shao-Horn, A. Wattiaux, L. Fournés, C. Delmas, Chem. Mater. 17 (2005) 4653–4659.
[50] S. Angelov, C. Friebel, E. Zhecheva, R. Stoyanova, J. Phys. Chem. Solids 53 (1992) 443–448.
[51] E. Gaudin, F. Taulelle, R. Stoyanova, E. Zhecheva, R. Alcántara, P. Lavela, J.L. Tirado, J. Phys. Chem. B 105 (2001) 8081–8087.
[52] G. Scholz, R. Stösser, J. Klein, G. Silly, J.Y. Buzaré, Y. Laligant, B. Ziemer, J. Phys.: Condens. Matter 14 (2002) 2101–2117.